Hindawi
Advances in Civil Engineering
Volume 2020, Article ID 4340381, 14 pages
https://doi.org/10.1155/2020/4340381

Research Article

Analytical Solution for Lateral-Torsional Buckling of Concrete-Filled Tubular Flange Girders with Torsional Bracing

Yingchun Liu,[1] **Zhaoming Hang**,[1] **Wenfu Zhang**,[1,2] **Keshan Chen**,[1] **and Jing Ji**[1]

[1]*College of Civil and Architecture Engineering, Northeast Petroleum University, Heilongjiang Key Laboratory of Disaster Prevention, Mitigation and Protection Engineering, No. 99 XueFu Road, Daqing 163318, China*
[2]*School of Architecture Engineering, Nanjing Institute of Technology, Nanjing 211167, China*

Correspondence should be addressed to Yingchun Liu; chunliuying@163.com

Received 25 July 2019; Accepted 20 December 2019; Published 27 January 2020

Academic Editor: Khalid Abdel-Rahman

Concrete-filled tubular flange girders have been used in bridges, and torsional bracings are widely used in them to increase the lateral-torsional buckling strength. This article proposes an analytical solution for the lateral-torsional buckling (LTB) of concrete-filled tubular flange steel girders with torsional bracing under a concentrated load. The modal trial functions of lateral displacement and the torsional angle are expressed by the first six terms of the trigonometric function. By introducing dimensionless parameters, the variational solution of energy for the buckling equation of the LTB of the girders is obtained, and the formula for the dimensionless critical moment of its LTB is derived using 1stOpt based on 32,550 data sets. Compared with the finite element method, the proposed critical formula is highly accurate and can be applied to engineering design. Finally, parametric studies were conducted on the effects of the stiffness of torsional bracing, the span of the girder, and the flange steel ratio.

1. Introduction

With rapid developments in construction and highway technologies, conventional steel I-girders do not have sufficient bearing capacity and stability to satisfy the demands of modern structures. Thus, hollow tubular flange steel girders and concrete-filled tubular flange steel girders (see Figure 1) have been researched. Compared with the I-section (open section), the tubular flange section has high torsional and compressive resistance. A number of researchers have investigated the behavior of hollow tubular flange steel girders and concrete-filled tubular flange steel girders (CFTFGS). Sause et al. conducted experimental studies on concrete-filled steel tubular flange girders and showed that they exhibit good lateral-torsional buckling capacity [1]. Kim and Sause also conducted finite element research and a parametric study on concrete-filled flange tubular flange girders to investigate the effects of sectional geometry and properties of the material on their lateral-torsional buckling strength and obtained formulae for their flexural strength [2]. Dong and Sause conducted a finite element study on the influence of stiffeners, geometric imperfections, residual stresses, cross-sectional dimensions, and the distribution of the bending moment on the LTB strength of HTFGS [3]. Hassanein and Kharoob conducted an analytical study on the shear behavior of transversely stiffened hollow tubular flange plate girders with rectangular tubes [4]. They also examined the global buckling resistance of hollow tubular flange plate girders [5]. Sause conducted experiments on straight and horizontally curved tubular flange girders, compared the results with those of a finite element analysis, and thus demonstrated the advantages of this type of girder [6]. Shao and Wang proposed a rectangular concrete-filled tubular flange and corrugated web girders, and they investigated their behavior under a concentrated load in the midspan. They found that the girders failed owing to flexural buckling and obtained the relevant theoretical equations [7]. Wang et al. conducted an experiment to examine the flexural behavior of a concrete composite girder with double tubular flanges and deduced the simplified formulae for flexural capacity [8]. Pan et al. studied

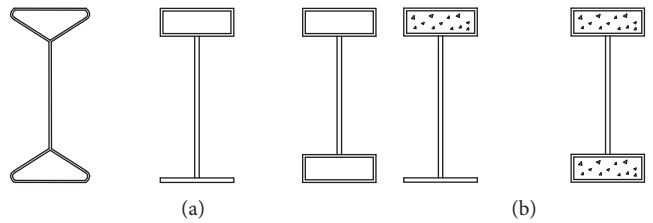

Figure 1: Girders with tubular flange. (a) Hollow tubular flange. (b) Concrete-filled tubular flange.

the behavior of square concrete-filled tubular columns with different penetrating gusset plates both experimentally and numerically [9].

Torsional bracings have been used in conventional steel I-girders to increase LTB capacity. Tong and Chen were the first to conduct a detailed theoretic analysis of the buckling behavior of simply supported girders under uniform moment and presented relative formulae for the required critical stiffness [10]. Valentino et al. investigated the effects of central elastic torsional restraints on the inelastic flexural-torsional buckling of steel I-girders [11]. Khelil and Larue conducted a detailed theoretic analysis featuring the matrices of rigidities and eigenvalues and showed that the effects of the distribution of moment and continuous restraints were weak [12]. Nguyen et al. used the energy method to obtain an analytical solution for the lateral-torsional buckling strength and stiffness requirements of I-girders with discrete torsional bracings [13]. Nguyen et al. proposed an analytical solution for the elastic flexural-torsional buckling stiffness requirements of I-girders with discrete torsional bracing under various loading conditions. They carried out a nonlinear finite element analysis featuring the initial imperfection and residual stress [14]. Mohammadi et al. investigated the lateral-torsional buckling strength and bracing stiffness requirements of monosymmetric I-girders with torsional bracing under pure bending conditions and proposed an energy-based approach to obtain the analytical solution [15].

From the above literature review, it is clear that the research on the stability-related behaviors of hollow tubular flange steel girders, concrete-filled tubular flange steel girders, and I-girders with torsional bracing is relatively mature. However, work on the lateral-torsional buckling behavior of concrete-filled tubular flange girders with torsional bracing is scarce. Nowadays, high-rise structures and tall bridges with a large span, large inner space, and irregular shapes are prevalent in construction. Requirements on the stability and strength of these structures are increasingly stringent. Cross beams have been applied to tubular flange girder bridges (see Figure 2) [6], which can act as a torsional bracing system. Torsional bracing can increase the strength and stability of concrete-filled tubular flange steel girders. Research on the behavior of CFTFGS with torsional bracing is thus important. This article uses the biaxial, symmetric concrete-filled rectangular tubular flange, simply supported girders with torsional bracing under a concentrated load as an example, and uses the energy variational method to establish equations of total potential energy. Through a series

Figure 2: A two-span straight tubular flange steel girder bridge of Tionesta Creek in Forest County, PA, USA.

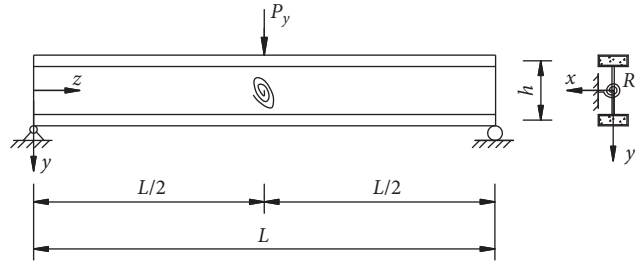

Figure 3: Calculation diagram of simply supported CFTFGS with torsional bracing under point load.

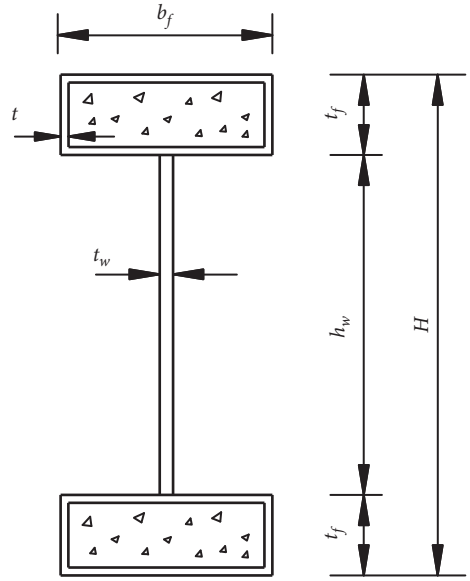

Figure 4: Diagram of section parameters.

of derivations, the formula for the dimensionless critical moment is obtained, and a large amount of data are acquired based on it. The regression formula for the stiffness requirement is then presented, and the formula for the critical moment of the lateral-torsional buckling of the CFTFGS under a concentrated load is obtained by nonlinear regression using 1stOpt software. The proposed formula is verified by the finite element method, and the results show that it is highly accurate. It is also clear that torsional bracing leads to a significant increase in the critical moment of the girders. Finally, parametric studies were conducted on the effects of the stiffness of the torsional bracing, the entire span of the girder, and the flange steel ratio.

2. Energy Variational Solution

This article analyzes the lateral-torsional buckling of simply supported CFTFGS with torsional bracing under a concentrated load. The torsional bracing was arranged at the midspan, and the diagram used for the calculation is shown in Figure 3. L is the length of the girder, P_y is the concentrated load, h is the distance between the centroid of the two flanges, and R is the stiffness of torsional bracing. The sectional parameters are shown in Figure 4, where H is the height of the section, b_f is the width of the flange, t_f is its height, t_w is the thickness of the web, h_w is its height, and t is the thickness of the tube.

The lateral-torsional deformation of the simply supported CFTFGS with torsional bracing is shown in Figure 5, where u is the lateral displacement of the section, θ is its torsion angle, a is the load position parameter, S is the section's shear center, and O is its centroid. Because the section is biaxial symmetric, the shear center and centroid coincide.

2.1. Basic Assumptions

(1) Hypothesis of rigid cross section: the contour of the cross section is nondeformable, i.e., it is rigid following the lateral-torsional buckling of the girder. This is the well-known peripheral rigidity hypothesis of Vlasov, which means that the local and distortional buckling are excluded from the LTB model.

(2) Hypothesis of neglecting shear deformation: the deformation owing in-plane bending and that owing to out-of-plane bending, and the torsion of each flat plate (either a web or the flanges) can be described by the Euler beam model and Kirchhoff plate model, respectively.

(3) The effect of the in-plane deformation on the strength of the LTB is ignored.

(4) The stress-strain relationship of steel follows Hooke's law [16–19].

2.2. Total Potential Energy. If there is no torsional bracing, the total potential energy of the simply supported CFTFGS girder under concentrated load can be expressed as follows [17–19]:

$$\Pi = \frac{1}{2}\int_0^L \left[\left(\mathrm{EI}_y\right)_{\mathrm{comp}} u''^2 + \left(\mathrm{EI}_\omega\right)_{\mathrm{comp}} \theta''^2 + \left(\mathrm{GJ}_k\right)_{\mathrm{comp}} \theta'^2 - 2M_x u''\theta\right] \mathrm{d}z - \frac{1}{2}\sum P_{yi}\left(a_i + \beta_x\right)\theta_i^2, \tag{1}$$

where M_x is the moment of the girder under concentrated load. The section is biaxial symmetric, the value of Wagner's coefficient β_x is zero, $(\mathrm{EI}_y)_{\mathrm{comp}}$ is the flexural rigidity along the minor axis, $(\mathrm{EI}_\omega)_{\mathrm{comp}}$ is the restrained torsional stiffness, $(\mathrm{GJ}_k)_{\mathrm{comp}}$ is the torsional rigidity of the open closed composite section. a_i is the distance between the location of the concentrated load P_{yi} and the section's centroid.

Because the cross section is the open closed composite section, previous theories could not solve the problem accurately and its characteristic parameters cannot be written directly as those of the thin-walled steel I-girder. Therefore, the formulae for $(\mathrm{EI}_y)_{\mathrm{comp}}$, $(\mathrm{EI}_\omega)_{\mathrm{comp}}$, and $(\mathrm{GJ}_k)_{\mathrm{comp}}$ are derived by the plate-beam theory proposed Zhang [20–23] and can be expressed as

$$\begin{aligned}
\left(\mathrm{EI}_y\right)_{\mathrm{comp}} &= \left(\frac{E_s}{1-\mu s^2}\right)\left(\frac{h_w t_w^3}{12}\right) + 2\left(E_s\left(\frac{t_f b_f^3}{12} - \frac{t_{fc} b_{fc}^3}{12}\right) + E_c\left(\frac{t_{fc} b_{fc}^3}{12}\right)\right),\\
\left(\mathrm{EI}_\omega\right)_{\mathrm{comp}} &= E_s\left(\frac{h_w^3 t_w^3}{144}\right) + 2\left(\frac{h}{2}\right)^2\left(E_s\left(\frac{t_f b_f^3}{12} - \frac{t_{fc} b_{fc}^3}{12}\right) + E_c\left(\frac{t_{fc} b_{fc}^3}{12}\right)\right),\\
\left(\mathrm{GJ}_k\right)_{\mathrm{comp}} &= \mathrm{GJ}_{\mathrm{kweb}} + \mathrm{GJ}_{\mathrm{kflange}},\\
\mathrm{GJ}_{\mathrm{kweb}} &= \frac{E_s}{2\left(1+\mu_s\right)}\left(\frac{h_w \times t_w^3}{3}\right),\\
\mathrm{GJ}_{\mathrm{kflange}} &= t_f^4 \cdot \frac{E_s}{2\left(1+\mu_s\right)}\left(0.8206\frac{2s^2}{r^2(r+s)} - 0.3649\frac{1}{r^2} + \frac{3r^4s^3 + 32r^2s^5 + 3s^7}{9mr^7 + 126mr^5s^2 + 126mr^3s^4 + 9mrs^6}\right),
\end{aligned} \tag{2}$$

where $t_{fc} = t_f - 2t$, $b_{fc} = b_f - 2t$, $r = t_f/t$, $s = b_f/t$, $m = G_s/G_c$, E_s is the elastic modulus of steel, E_c is the elastic modulus of concrete, μ_s is the value of Poisson's ratio of steel, G_s is the value of the shear modulus of steel, and G_c is the value of the shear modulus of concrete.

The total potential energy of torsional bracing can be expressed as

$$\Pi_2 = \frac{1}{2}R\left[\theta\left(\frac{L}{2}\right)\right]^2. \tag{3}$$

2.3. Displacement Function. The displacement function and angle function of six trigonometric series can be expressed as

$$u(z) = \sum_{i=1}^{6} A_i h \sin\left(\frac{i\pi z}{L}\right), \tag{4}$$

$$\theta(z) = \sum_{i=1}^{6} B_i \sin\left(\frac{i\pi z}{L}\right) \tag{5}$$

where h is the distance between the centroid of the two flanges, and A_i and B_i are undetermined dimensionless constants.

The displacement function satisfies the boundary condition of the simply supported girder

$$\begin{aligned} &u(0) = u(L) = 0; \quad u''(0) = u''(L) = 0, \\ &\theta(0) = \theta(L) = 0; \quad \theta''(0) = \theta''(L) = 0. \end{aligned} \tag{6}$$

2.4. Moment Function. The moment function of the simply supported girder under concentrated load can be expressed as

$$M_x(z) = \frac{P_y}{2}\left|z - \frac{L}{2}\right| - \frac{P_y L}{4} \quad 0 \le z \le L. \tag{7}$$

By substituting equations (4)–(7) into equation (1), the total potential energy with no bracing can be expressed as

$$\Pi_1 = \frac{1}{2}\left(\frac{\pi^4 h^2 A_1^2 \left(\mathrm{EI}_y\right)_{\mathrm{comp}}}{2L^3} + \frac{\pi^4 B_1^2 \left(\mathrm{EI}_\omega\right)_{\mathrm{comp}}}{2L^3} + \frac{\pi^2 B_1^2 \left(\mathrm{GJ}_k\right)_{\mathrm{comp}}}{2L} - \frac{\left(\pi^2 + 4\right) A_1 B_1 h P_y}{8} - a B_1^2 P_y\right), \tag{8}$$

where a is the distance between the location of the concentrated load P_y and the section's centroid.

By substituting equation (5) into equation (3), the potential energy of the bracing can be expressed as

$$\Pi_2 = \frac{1}{2}R\left[B_1 - B_3 + B_5\right]^2. \tag{9}$$

Thus, the total potential energy of the simply supported girder with torsional bracing under concentrated load can be expressed as

$$\Pi = \Pi_1 + \Pi_2 = \frac{1}{2}\left(\frac{\pi^4 h^2 A_1^2 \left(\mathrm{EI}_y\right)_{\mathrm{comp}}}{2L^3} + \frac{\pi^4 B_1^2 \left(\mathrm{EI}_\omega\right)_{\mathrm{comp}}}{2L^3} + \frac{\pi^2 B_1^2 \left(\mathrm{GJ}_k\right)_{\mathrm{comp}}}{2L} - \frac{\left(\pi^2 + 4\right) A_1 B_1 h P_y}{8} - a B_1^2 P_y\right) + \frac{R}{2}\left(B_1 - B_3 + B_5\right)^2. \tag{10}$$

2.5. Dimensionless Buckling Equation. According to theory of the minimum of total potential energy [17], we get

$$\begin{aligned} &\frac{\partial \prod}{\partial A_i} = 0, \quad i = 1, 2, 3, 4, 5, 6, \\ &\frac{\partial \prod}{\partial B_i} = 0, \quad i = 1, 2, 3, 4, 5, 6. \end{aligned} \tag{11}$$

We then define the dimensionless parameters, which are given as follows [16, 24–29]:

$$\begin{aligned} \widetilde{M}_{\mathrm{cr}} &= \frac{M_{\mathrm{cr}}}{\left(\pi^2 \left(\mathrm{EI}_y\right)_{\mathrm{comp}}/L^2\right)h}; \\ \widetilde{a} &= \frac{a}{h}; \\ \widetilde{R} &= \frac{\pi \mathrm{RL}^3}{\left(\mathrm{EI}_y\right)_{\mathrm{comp}} h^2}; \\ K &= \sqrt{\frac{\pi^2 \left(\mathrm{EI}_\omega\right)_{\mathrm{comp}}}{\left(\mathrm{GJ}_k\right)_{\mathrm{comp}} L^2}}; \\ S &= \frac{\left(\mathrm{EI}_y\right)_{\mathrm{comp}} h^2}{\left(\mathrm{EI}_\omega\right)_{\mathrm{comp}}}; \\ P_y &= \frac{4M_{\mathrm{cr}}}{L}, \end{aligned} \tag{12}$$

where M_{cr} is the critical moment of flexural buckling of CFTFGS, $\widetilde{M}_{\mathrm{cr}}$ is the dimensionless critical moment of lateral buckling of CFTFGS, $\widetilde{a}$ is the dimensionless loading position, $\widetilde{R}$ is the dimensionless stiffness of torsional bracing, K is the torsional parameter, and S is a parameter introduced to characterize the relationship between restrained torsional stiffness and flexural stiffness around the minor axis.

Multiplying equation (11) by $(L^3/\mathrm{EI}_y h^2)$ and substituting equation (12) into equation (11), the dimensionless buckling equation can be obtained, and it is expressed in matrix form as follows:

$$\begin{bmatrix} {}^0R & {}^0S \\ {}^0T & {}^0Q \end{bmatrix}\begin{bmatrix} A \\ B \end{bmatrix} = \widetilde{M}_{cr}\begin{bmatrix} {}^1R & {}^1S \\ {}^1T & {}^1Q \end{bmatrix}\begin{bmatrix} A \\ B \end{bmatrix}, \tag{13}$$

where the elements of the subblock matrix are expressed as

$$
{}^{0}R = \begin{bmatrix}
\frac{\pi^4}{2} & 0 & 0 & 0 & 0 & 0 \\
 & 8\pi^4 & 0 & 0 & 0 & 0 \\
 & & \frac{81\pi^4}{2} & 0 & 0 & 0 \\
 & & & 128\pi^4 & 0 & 0 \\
 & \text{symmetric} & & & \frac{625\pi^4}{2} & 0 \\
 & & & & & 648\pi^4
\end{bmatrix},
$$

$$
{}^{0}S = \begin{bmatrix}
0 & 0 & 0 & 0 & 0 & 0 \\
0 & 0 & 0 & 0 & 0 & 0 \\
0 & 0 & 0 & 0 & 0 & 0 \\
0 & 0 & 0 & 0 & 0 & 0 \\
0 & 0 & 0 & 0 & 0 & 0 \\
0 & 0 & 0 & 0 & 0 & 0
\end{bmatrix},
$$

$${}^{0}T = {}^{0}S,$$

$$
{}^{0}Q = \begin{bmatrix}
\frac{\pi^4}{2S} + \frac{\pi^4}{2SK^2} + \frac{4\tilde{R}}{\pi S} & 0 & -\frac{4\tilde{R}}{\pi S} & 0 & \frac{4\tilde{R}}{\pi S} & 0 \\
 & 2\pi^4 + \frac{\pi^4}{2K^2} & 0 & 0 & 0 & 0 \\
 & & \frac{81\pi^4}{2S} + \frac{9\pi^4}{2SK^2} + \frac{4\tilde{R}}{\pi S} & 0 & -\frac{4\tilde{R}}{\pi S} & 0 \\
 & & & 32\pi^4 + \frac{2\pi^4}{K^2} & 0 & 0 \\
 & \text{symmetric} & & & \frac{625\pi^4}{2S} + \frac{25\pi^4}{2SK^2} + \frac{4\tilde{R}}{\pi S} & 0 \\
 & & & & & 162\pi^4 + \frac{9\pi^4}{2K^2}
\end{bmatrix},
$$

$$
{}^{1}R = \begin{bmatrix}
0 & 0 & 0 & 0 & 0 & 0 \\
0 & 0 & 0 & 0 & 0 & 0 \\
0 & 0 & 0 & 0 & 0 & 0 \\
0 & 0 & 0 & 0 & 0 & 0 \\
0 & 0 & 0 & 0 & 0 & 0 \\
0 & 0 & 0 & 0 & 0 & 0
\end{bmatrix},
$$

$$
{}^{1}S = \begin{bmatrix}
\pi^2 + \frac{\pi^4}{4} & 0 & -\pi^2 & 0 & \frac{\pi^2}{9} & 0 \\
0 & \pi^4 & 0 & -\frac{32\pi^2}{9} & 0 & 0 \\
-9\pi^2 & 0 & \pi^2 + \frac{9\pi^4}{4} & 0 & -9\pi^2 & 0 \\
0 & -\frac{128\pi^2}{9} & 0 & 4\pi^4 & 0 & -\frac{384\pi^2}{25} \\
\frac{25\pi^2}{9} & 0 & -25\pi^2 & 0 & \pi^2 + \frac{25\pi^4}{4} & 0 \\
0 & 0 & 0 & -\frac{864\pi^2}{25} & 0 & 9\pi^4
\end{bmatrix},
$$

$$
{}^{1}T = {}^{1}S^{T},
$$

$$
Q^{1} = \begin{bmatrix}
4\pi^2\tilde{a} & 0 & -4\pi^2\tilde{a} & 0 & 4\pi^2\tilde{a} & 0 \\
 & 0 & 0 & 0 & 0 & 0 \\
 & & 4\pi^2\tilde{a} & 0 & -4\pi^2\tilde{a} & 0 \\
 & & & 0 & 0 & 0 \\
 & \text{symmetric} & & & 4\pi^2\tilde{a} & 0 \\
 & & & & & 0
\end{bmatrix}. \tag{14}
$$

Therefore, the dimensionless critical moment $\tilde{M}_{cr}$ of the CFTFGS with torsional bracing can be obtained from the minimum eigenvalue of equation (13).

It is clear from the derivation that when $\tilde{a}$, $\tilde{R}$, S, and K are given, the dimensionless critical moment $\tilde{M}_{cr}$ can be obtained. By varying the size of the section, the span-to-height ratio, and dimensionless torsional bracing stiffness, different values of $\tilde{a}$, $\tilde{R}$, S, and K can be obtained. Therefore, a series of $\tilde{M}_{cr}$ can be obtained for the regression analysis of the formula for the dimensionless critical moment.

The value of the torsional parameter K varied from 0.05 to 0.35. A total of 500 sections were analyzed, and the values of K of many sections were found to be close. Thus, the data were selected according to increase in the value of K with a step size of 0.01, and 100 sections of different sizes and spans were finally chosen for regression analysis.

2.6. Regression Analysis. MATLAB software was used to write the program for calculating the dimensionless critical moment of the CFTFGS with the torsional bracing under concentrated load. By varying the values of $\tilde{a}$, $\tilde{R}$, S, and K, the value of $\tilde{M}_{cr}$ can be obtained. The results showed that once the value of $\tilde{R}$ had reached $\tilde{R}_T$, called the threshold stiffness of dimensionless torsional bracing, the value of $\tilde{M}_{cr}$ no longer increased. The relationship between them is shown in Figure 6. The value of $\tilde{R}_T$ varied as the girder changed. Thus, to obtain accurate data, 500 base sections were selected through multiple trials (the span L of each section could be changed), and the step size of $\tilde{R}$ was set to 200. Finally, 32,550 data sets were obtained for the regression of the formula for dimensionless critical moment.

The critical moment of the CFTFGS with torsional bracing was regressed by 1stOpt software by considering the effect of multiple parameters. The critical moment of the CFTFGS with torsional bracing can be expressed as

$$
\begin{aligned}
\tilde{M}_{cr} = {} & c_1\tilde{M}_{cr0} + c_2\left(\tilde{M}_{crT} - \tilde{M}_{cr0}\right)\left(\frac{\tilde{R}}{\tilde{R}_T}\right)^{0.995} \\
& \cdot \left[1 + c_3\left(\frac{\tilde{R}}{\tilde{R}_T}\right) - c_4\left(\frac{\tilde{R}}{\tilde{R}_T}\right)^2 + c_5\left(\frac{\tilde{R}}{\tilde{R}_T}\right)^3 + c_6\left(\frac{\tilde{R}}{\tilde{R}_T}\right)^4\right], \\
& 0 < \tilde{R} < \tilde{R}_T,
\end{aligned} \tag{15}
$$

where $\tilde{M}_{cr0}$ is the critical moment without torsional bracing, and it can be expressed as

$$
\tilde{M}_{cr0} = \beta_1\left[\beta_2\tilde{a} + \beta_3K^{-1} + \sqrt{(\beta_2\tilde{a})^2 + S(1 + K^{-2}) + \beta_4K^{-1}}\right], \tag{16}
$$

where $\tilde{M}_{crT}$ is the dimensionless critical moment of the CFTFGS with torsional bracing when $\tilde{R}$ reaches $\tilde{R}_T$, and it can be expressed as

$$
\begin{aligned}
\tilde{M}_{crT} = {} & \beta_{1T}\left[\beta_{2T}\tilde{a} + \beta_{3T}K^{-1} + \beta_{4T}\tilde{R}_T^{1/3}\right. \\
& \left. + \sqrt{(\beta_{2T}\tilde{a})^2 + S(1 + K^{-2}) + \beta_{5T}K^{-1}}\right],
\end{aligned} \tag{17}
$$

where the threshold stiffness of dimensionless torsional bracing $\tilde{R}_T$, which can be expressed as

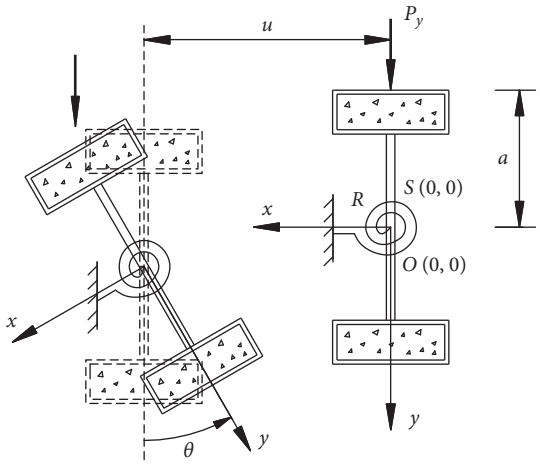

Figure 5: Lateral-torsional deformation of simply supported CFTFGS with torsional bracing.

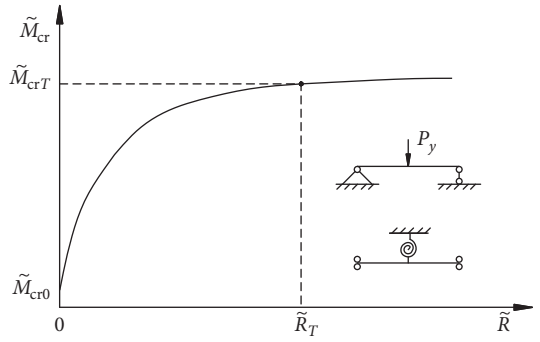

Figure 6: Relationship between dimensionless critical moment and dimensionless torsional stiffness.

Table 1: The values of parameters of critical moment with torsional bracing $\widetilde{M}_{cr}$ (equation (15)).

Parameter	c_1	c_2	c_3	c_4	c_5	c_6
Value	1.047	2.128	−0.816	−0.137	0.299	−0.159

Table 2: The values of parameters of critical moment with no torsional bracing $\widetilde{M}_{cr0}$ (equation (16)).

Parameter	β_1	β_2	β_3	β_4
Value	0.213	−4.086	1.153	1.127

Table 3: The values of parameters of critical moment $\widetilde{M}_{crT}$ (equation (17)).

Parameter	β_{1T}	β_{2T}	β_{3T}	β_{4T}	β_{5T}
Value	−0.706	0.126	−4.780	0.141	−11.265

Table 4: The values of parameters of the threshold stiffness of dimensionless torsional bracing (equation (18)).

N	γ_1	γ_2	m_1	m_2	n_1	n_2
Value	103.284	10896.680	0.002	0.643	0.069	53.908

Table 5: The correlation coefficients of each formula.

Equation	Equation (14)	Equation (15)	Equation (16)	Equation (17)
Correlation coefficient	0.999901	0.999998	0.999999	0.999961

Table 6: The valid applicable ranges of parameters in the formulae.

	L/H	b_f/t_f	$\bar{a}$	S	K
Range	8~30	1.1~2.7	0.565~0.666	4	0.05~0.35

$$\widetilde{R}_T = \frac{2\pi\left(8+\alpha_1\right)\sqrt{4+\alpha_2}}{\alpha_3}, \tag{18}$$

where $\alpha_1 = \gamma_1 K^{-4} + \gamma_2 K^{-1} S^{-1}$, $\alpha_2 = m_1 K^{-4} + m_2 K^{-1} S^{-1}$, $\alpha_3 = n_1 K^{-4} + n_2 K^{-1} S^{-1}$.

The value of each parameter in the above formulae are shown in Tables 1–4, and their correlation coefficients are shown in Table 5. The correlation coefficients were close to one, which means that the fitting precisions of the formulae were high.

Note that the tube section of the CFTFGS was determined according to the cold-drawn-shaped steel tubes (GB/T3094-2012) [30]. To minimize web distortion, the ratio of the height of the web to its thickness needed to meet the following requirement [31]is given as

$$\frac{h_w}{t_w} \le 11\left(\frac{E_s}{f_y}\right)^{1/3}, \tag{19}$$

where, f_y is the yield stress of steel.

The parameters above are based on the results of regression. Thus, the valid applicable range of the parameters in equations (15) to (18) is listed in Table 6.

3. Numerical Modeling Study

3.1. Finite Element Model

3.1.1. Types of Finite Element Model. ANSYS software was used to simulate the lateral-torsional buckling behavior of the CFTFGS with torsional bracing. The steel material of the web and steel tubes are modeled using SHELL181 element. This element is a thin, shear flexible, isoparametric quadrilateral shell with four nodes and six degrees of freedom for each node. To improve accuracy, the value of KEYOPT(3) was set to two. The concrete material is modeled using the SOLID45 element defined by eight nodes with three degrees of freedom at each node. To establish contact between the steel tube and concrete, the SECOFFSET command was used to offset nodes of the shell element to the inner surface of the steel tube. The CONTA173 element was selected as contact element. To obtain the bonded behavior of the contact surface, the value of KEYOPT(12) was set to five. TARGE170 element was selected as target element. To generate multipoint constrains (MPC), the value of KEYOPT(5) was set to two. According to the stiffness of the materials, the inner surface of the steel tube was defined as the target surface and

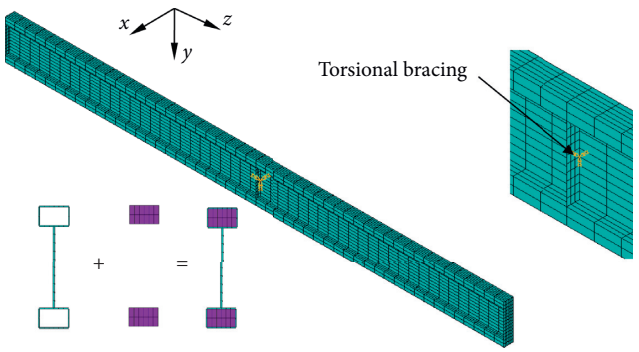

Figure 7: FEM model of the concrete-filled tubular flange girder with torsional bracing.

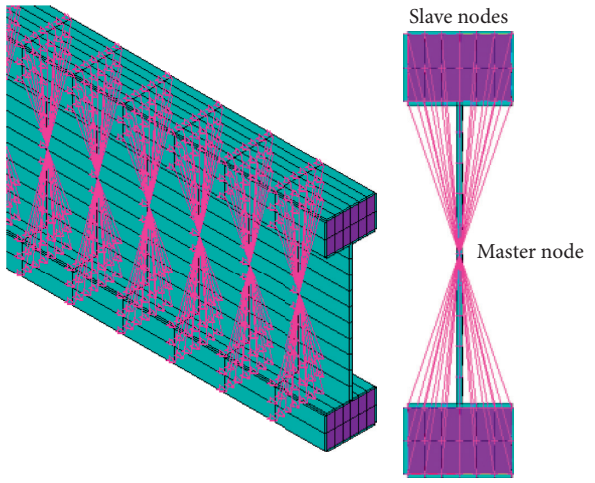

Figure 8: Rigid peripheral applications along the length of girder (constraint rotation around z-axis). (a) Rigid peripheral applications. (b) Master and slave nodes.

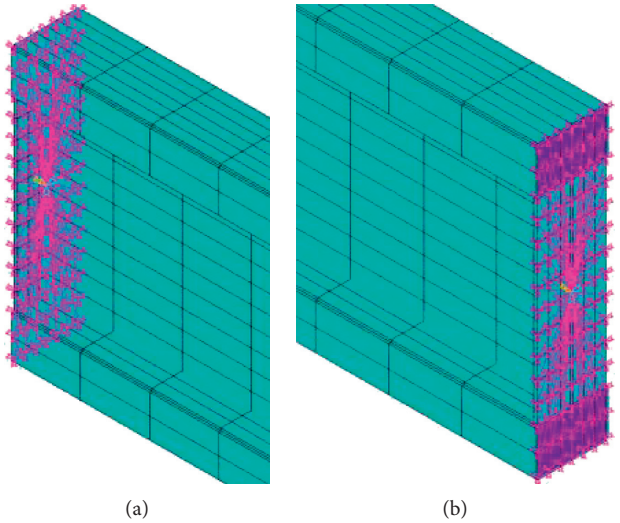

Figure 9: Boundary conditions. (a) Left end support. (b) Right end support.

Table 7: The sizes of the sections.

Parameter	H (mm)	b_f (mm)	t_f (mm)	t (mm)	t_w (mm)	L (mm)
Section 1	500	100	60	3	6	16000
Section 2	300	60	40	2	3	10000

the concrete surface as the contact surface. The ESURF command was used to generate the target element and contact element.

Torsional bracing was modeled using the spring element COMBIN14, which has longitudinal and torsional capability in one-, two-, and three-dimensional (3D) applications. The value of KEYOPT(2) was set to four. Then, the spring element was defined as 1D element with a degree of freedom of rotation about the z-axis [32, 33]. The rotational stiffness R was defined by a real constant, and the rotational spring element was attached at the shear center (centroid center) of the section at the midspan.

3.1.2. Material Model and Meshing Considerations. In the elastic lateral-torsional buckling analysis, steel and concrete were assumed to be perfectly elastic materials, where the elastic modulus of steel $E_s = 2.06 \times 10^5$ MPa and Poisson's ratio $\mu_s = 0.3$, and the elastic modulus of concrete $E_c = 3.25 \times 10^4$ MPa and Poisson's ratio $\mu_c = 0.2$. To ensure accuracy, different mesh sizes were considered. The flanges and web were divided into 50 parts along the span. The web was divided into 10 parts along the height. Then, widths of the steel tube and in-filled concrete were divided into six parts, and their heights into two parts. Thus, the elements of steel tube and in-filled concrete had identical node coordinates, and contact pairs could be established at their interface. The finite element model of the CFTFGS with torsional bracing is shown in Figure 7.

To prevent local buckling of loading at the midspan, stiffeners were set in the midspan and the two ends. The CERIG command was used to satisfy the requirement of a rigid periphery. In other words, the constraint equation around the z-axis is established for each section along the span to ensure that the shape of the section remained unchanged after deformation. The rigid peripheral applications are shown in Figure 8.

3.1.3. Boundary Conditions. To satisfy the ideal clamping support boundary condition, the CERIG command was used to establish the rigid peripheral region. The master node was the centroid of the end section, and the slave nodes consisted of other nodes of the end section. The master nodes of the left and right ends were restrained against in-plane vertical deflection (*uy*), out-of-plane horizontal deflection (*ux*), and twisting rotation (*rotz*) but unrestrained against in-plane rotation (*rotx*), rotation (*roty*) around the minor axis, and warping displacement. Furthermore, only the master node of the left end was restrained against longitudinal horizontal displacement (*uz*). The boundary conditions are shown in Figure 9.

Table 8: Comparison of theoretical analysis and finite element analysis.

Section 1				Section 2			
$\tilde{R}$	M_{cr} (FEM) (kN·m)	M_{cr} (equation (15)) (kN·m)	Error (%)	$\tilde{R}$	M_{cr} (FEM) (kN·m)	M_{cr} (equation (15)) (kN·m)	Error (%)
0	122.16	121.00	−0.96	0	30.84	30.78	−0.20
1000	130.48	129.41	−0.83	1000	32.52	32.47	−0.16
2000	138.12	137.15	−0.71	2000	34.10	34.06	−0.12
3000	145.19	144.41	−0.54	4000	36.97	37.00	0.06
4000	151.83	151.25	−0.38	6000	39.54	39.67	0.34
6000	164.00	163.86	−0.08	10000	43.98	44.40	0.96
10000	184.35	185.73	0.74	12000	45.92	46.52	1.28
15000	204.91	208.49	1.72	15000	48.58	49.45	1.76
20000	221.48	227.57	2.68	17000	50.20	51.25	2.05
25000	235.41	243.85	3.46	20000	52.41	53.77	2.53
30000	246.73	257.90	4.33	25000	55.64	57.54	3.31
40000	265.32	280.84	4.96	30000	58.39	60.86	4.05
50000	278.68	298.61	5.53	40000	62.88	66.43	5.34
60000	289.39	306.01	6.13	50000	66.36	70.90	6.41
70000	297.74	312.49	6.67	60000	69.12	74.54	7.27
80000	304.51	332.92	7.09	70000	71.38	77.55	7.96
85000	307.30	336.83	7.39	80000	73.09	80.05	8.70
87102*	310.11	337.14	7.70	100000	75.99	83.93	9.47
95000	312.49	337.14	8.05	110267*	78.02	85.11	8.33
100000	314.46	337.14	8.32	130000	79.50	85.11	6.60

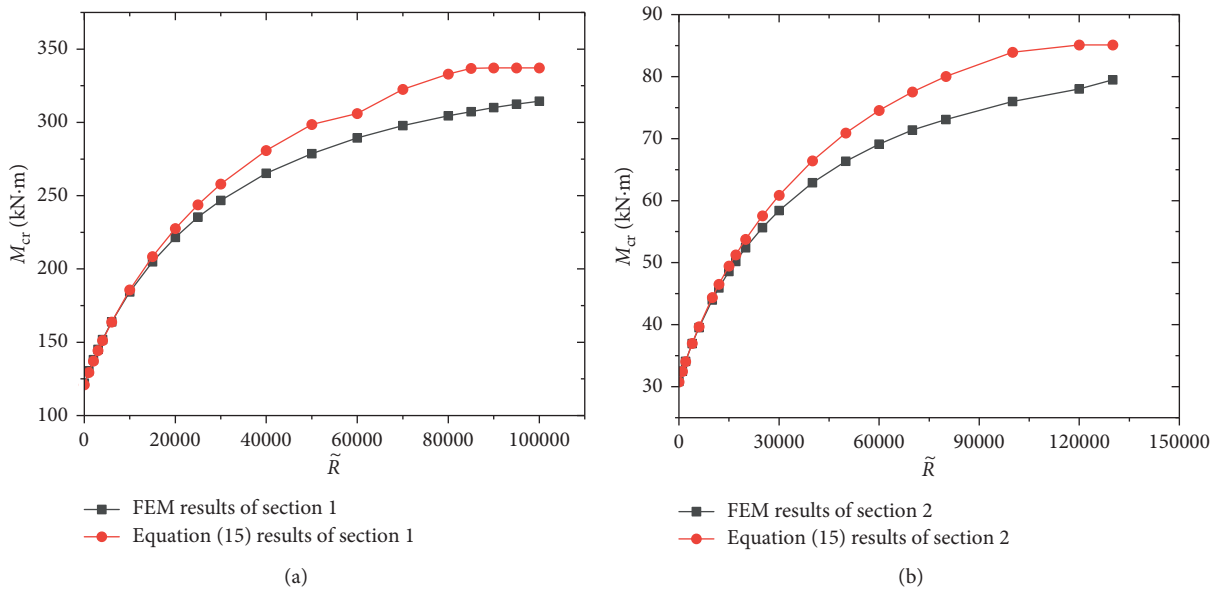

Figure 10: Relationship between critical moments and dimensionless torsional bracing stiffness. (a) Section 1. (b) Section 2.

Table 9: The sizes of the three sections.

Parameter	H (mm)	b_f (mm)	t_f (mm)	t (mm)	h_w (mm)	t_w (mm)
Section 1	440	160	80	3	280	4
Section 2	1260	500	300	6	660	8
Section 3	600	120	60	3	480	4

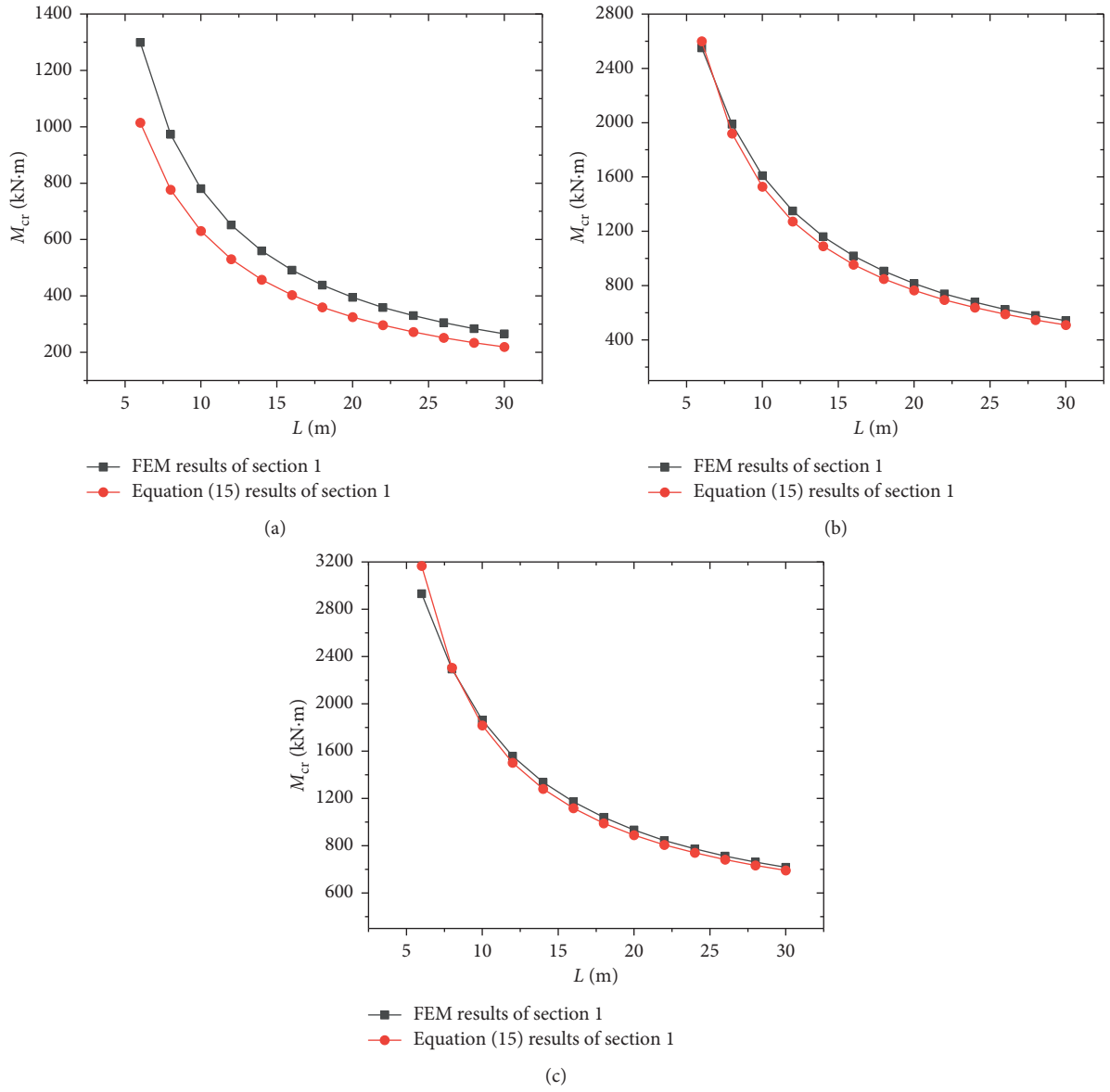

Figure 11: Relationship between critical moments and span (section 1). (a) $\widetilde{R} = 0$, (b) $\widetilde{R} = (1/2)\widetilde{R}_T$, (c) $\widetilde{R} = \widetilde{R}_T$.

3.2. Verification of Results. Two kinds of sections were selected for the buckling analysis of the eigenvalues, and the critical moment of finite element analysis was then calculated. The sizes of the two sections are shown in Table 7.

By varying the dimensionless stiffness of torsional bracing, a series of dimensionless critical moments were obtained. By $\pi^2 (\mathrm{EI}_y)_{\mathrm{comp}} h/L^2$, the dimension critical moments are listed in Table 8. The variations in critical moments with torsional bracing stiffness under a concentrated load are shown in Figure 10. $\widetilde{R}_T$ was obtained by equation (18) (marked with * in Table 8).

4. Parametric Study

4.1. Effect of $\widetilde{R}$. Sections 1 and 2 were used to study in the effects of $\widetilde{R}$, and the results of the finite element analysis and the analytical solution are shown in Figure 10.

It is clear that before the dimensionless stiffness of the torsional bracing $\widetilde{R}$ reaches $\widetilde{R}_T$, the critical moment of lateral-torsional buckling increased. Finally, it reached its maximum value. Therefore, torsional bracing can significantly increase the bending and torsion resistance, especially when the value of the stiffness of torsional bracing is not high.

4.2. Effect of Span (L). Hassanein and Silvestre found that structural torsional buckling behavior is affected by span (L) [34]. In this article, three sections were selected for a parametric study of the effect of the span (L). The parameters of the sections are shown in Table 9.

If the values of the stiffness of the torsional bracing are different, the span L may have different effects on the critical moment. We thus selected three values of the stiffness of

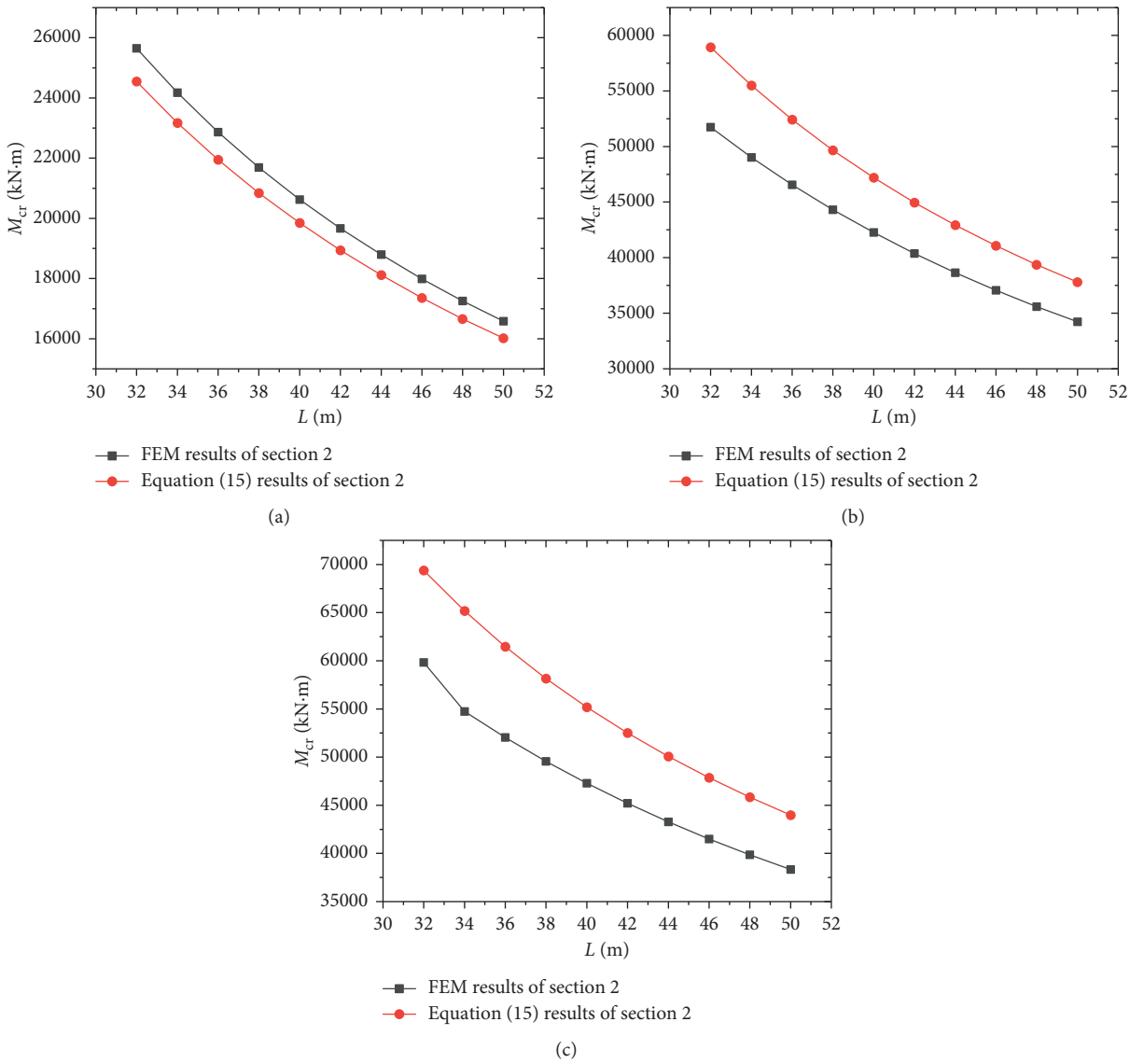

Figure 12: Relationship between critical moments and span (section 2). (a) $\widetilde{R} = 0$, (b) $\widetilde{R} = (1/2)\widetilde{R}_T$, (c) $\widetilde{R} = \widetilde{R}_T$.

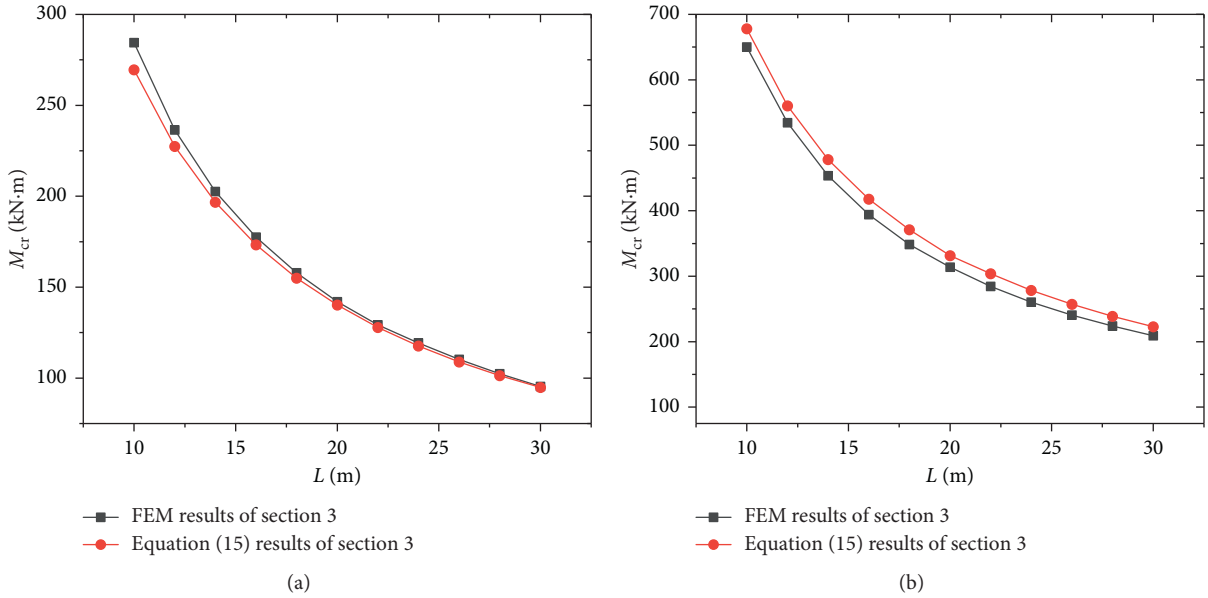

Figure 13: Continued.

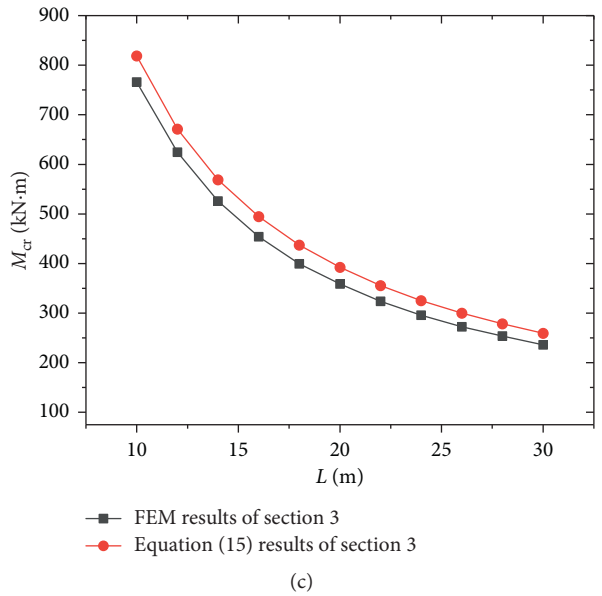

Figure 13: Relationship between critical moments and span (section 3). (a) $\widetilde{R} = 0$, (b) $\widetilde{R} = (1/2)\widetilde{R}_T$, (c) $\widetilde{R} = \widetilde{R}_T$.

Table 10: The sizes of the sections.

Parameter	H (mm)	b_f (mm)	t_f (mm)	t (mm)	h_w (mm)	t_w (mm)	Flange steel ratio (%)	L (mm)
Section 1	600	160	60	1.8	480	4	8.12	16000
Section 2	600	160	60	2.1	480	4	9.44	16000
Section 3	600	160	60	2.4	480	4	10.76	16000
Section 4	600	160	60	2.7	480	4	12.07	16000
Section 5	600	160	60	3.0	480	4	13.38	16000
Section 6	600	160	60	3.3	480	4	14.67	16000
Section 7	600	160	60	3.6	480	4	15.96	16000
Section 8	600	160	60	3.9	480	4	17.24	16000
Section 9	600	160	60	4.2	480	4	18.515	16000
Section 10	600	160	60	4.5	480	4	19.78	16000

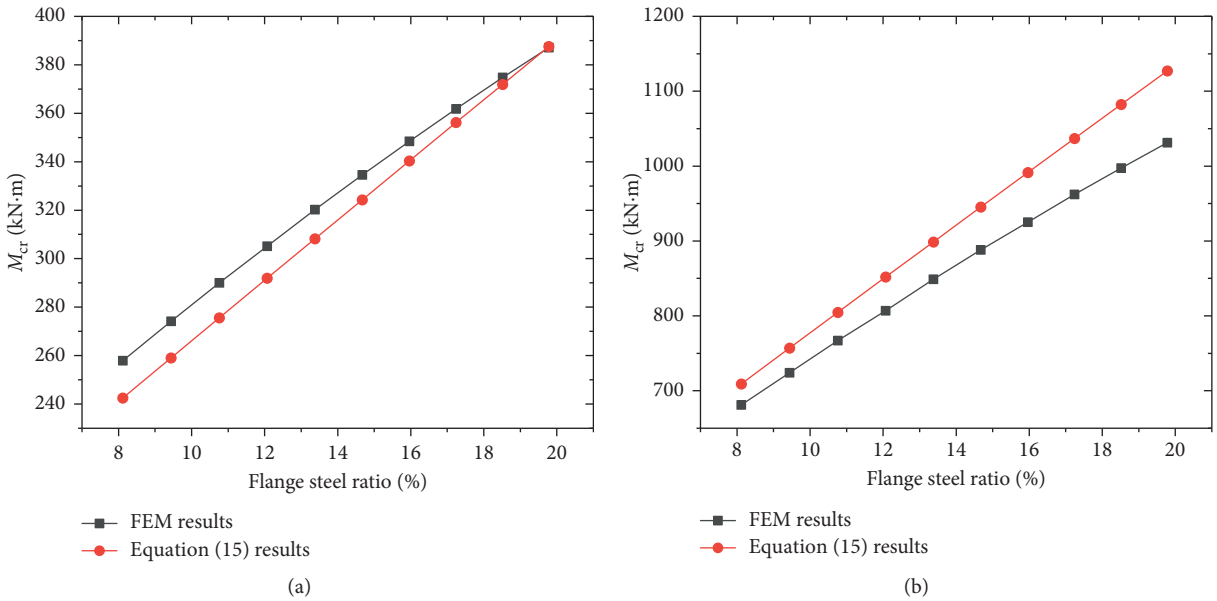

Figure 14: Relationship between critical moments and flange steel ratio. (a) $\widetilde{R} = 0$. (b) $\widetilde{R} = \widetilde{R}_T$.

torsional bracing ($\widetilde{R} = 0$, $\widetilde{R} = (1/2)\widetilde{R}_T$, $\widetilde{R} = \widetilde{R}_T$) for analysis ($\widetilde{R}_T$was obtained by equation (18)). A comparison of the results of the finite element analysis and the analytical solutions of equation (14) is shown in Figures 11~13.

From Figures 11~13, it is clear that the value of the critical moment decreased as span increased. The finite element analysis showed that there was no out-of-plane deformation when the span did not reach a certain value for each kind of girder, which means that lateral-torsional buckling did not occur in it.

4.3. Effect of Flange Steel Ratio. Ten sections with different flange steel ratios, ranging from 8.12% to 19.78%, were selected and divided into two groups that were different only in this ratio. The data of these sections are shown in Table 10.

To reflect the impact of torsional bracing, in the finite element analysis, two situations were studied when the girders' torsional bracing stiffness values were zero and $\widetilde{R}_T$. The results are shown in Figure 14.

From Figure 14, it is clear that the value of the critical moment increased with the steel ratio and the relationship between them was roughly linear. This suggests a stable relationship between the critical moment and the steel ratio. Thus, when the flexural and torsional capability of such girders need to be strengthened in engineering, increasing the steel ratio is a feasible solution.

5. Conclusions

This article focused on the torsional buckling of concrete-filled tubular flange girders (CFTFGS) with torsional bracing. Theoretical and finite element studies were conducted, and following conclusions can be drawn:

(1) The energy variational solution for the critical moment of the lateral-torsional buckling of a simply supported concrete-filled tubular flange girder with torsional bracing was derived. Formulae for $(EI_y)_{comp}$, $(EI_\omega)_{comp}$, and $(GJ_k)_{comp}$ of the open closed composite section were also given.

(2) Based on 32,550 sets of dimensionless data obtained from the solution of the dimensionless buckling equation, and using 1stOpt software, formulae for $\widetilde{M}_{cr}$, $\widetilde{M}_{cr0}$, $\widetilde{M}_{crT}$, and $\widetilde{R}_T$ were derived.

(3) A finite element model was established and compared with the analytical solution. The results show a good match between them. Thus, the proposed formula can be used as reference in engineering practice.

(4) By adding torsional bracing to the girders, the bending and torsional resistance of the CFTFGS can be significantly strengthened, and the growth rate of the critical moment decreases as the stiffness of the torsional bracing increases.

(5) When the span (L) of the girder ranged from 5 m to 50 m, the value of the critical moment decreased as the span increased, where the rate of decrease in the former declined as the latter increased. When the flange steel ratio ranged from 4.75% to 19.78%, the value of the critical moment increased with this ratio, and the relationship was roughly linear.

Data Availability

The data used to support the findings of this study are available from the corresponding author upon request.

Conflicts of Interest

The authors have no conflicts of interest to declare.

Acknowledgments

This work was supported by the National Natural Science Foundation of China (51578120 and 51178087), the Petro-China Innovation Foundation (2016D-5007-0608), the Graduate Innovation Project of Northeast Petroleum University (JYCX-CX05-2018), and Opening Fund for Key Laboratory of the Ministry of Education for Structural Disaster and Control of Harbin Institute of Technology (HITCE201908).

References

[1] R. Sause, B.-G. Kim, and M. R. Wimer, "Experimental study of tubular flange girders," *Journal of Structural Engineering*, vol. 134, no. 3, pp. 384–392, 2008.

[2] B.-G. Kim and R. Sause, "Lateral torsional buckling strength of tubular flange girders," *Journal of Structural Engineering*, vol. 134, no. 6, pp. 902–910, 2008.

[3] J. Dong and R. Sause, "Flexural strength of tubular flange girders," *Journal of Constructional Steel Research*, vol. 65, no. 3, pp. 622–630, 2009.

[4] M. F. Hassanein and O. F. Kharoob, "Shear strength and behavior of transversely stiffened tubular flange plate girders," *Engineering Structures*, vol. 32, no. 9, pp. 2617–2630, 2010.

[5] M. F. Hassanein and O. F. Kharoob, "Flexural strength of hollow tubular flange plate girders with slender stiffened webs under mid-span concentrated loads," *Thin-Walled Structures*, vol. 69, pp. 18–28, 2013.

[6] R. Sause, "Innovative steel bridge girders with tubular flanges," *Structure and Infrastructure Engineering*, vol. 11, no. 4, pp. 450–465, 2015.

[7] Y. Shao and Y. Wang, "Experimental study on static behavior of I-girder with concrete-filled rectangular flange and corrugated web under concentrated load at mid-span," *Engineering Structures*, vol. 130, pp. 124–141, 2017.

[8] C. S. Wang, J. W. Zhu, X. L. Zhai, X. P. Wang, and H. Liu, "Flexural behavior experiment of steel and concrete composite girder with double tubular flanges," *China Journal of Highway Transport*, vol. 30, no. 3, pp. 147–158, 2017.

[9] J. Pan, P. Wang, Y. Zheng, Z. Wang, and D. Liu, "An analytical study of square CFT columns in bracing connection subjected to axial loading," *Advances in Civil Engineering*, vol. 2018, Article ID 8618937, 15 pages, 2018.

[10] G. S. Tong and S. F. Chen, "Buckling of laterally and torsional braced beams," *Journal of Constructional Steel Research*, vol. 11, no. 1, pp. 41–55, 1988.

[11] J. Valentino, Y.-L. Pi, and N. S. Trahair, "Inelastic buckling of steel beams with central torsional restraints," *Journal of Structural Engineering*, vol. 123, no. 9, pp. 1180–1186, 1997.

[12] A. Khelil and B. Larue, "Simple solutions for the flexural-torsional buckling of laterally restrained I-beams," *Engineering Structures*, vol. 30, no. 10, pp. 2923–2934, 2008.
[13] C. T. Nguyen, J. Moon, V. N. Le, and H.-E. Lee, "Lateral-torsional buckling of I-girders with discrete torsional bracings," *Journal of Constructional Steel Research*, vol. 66, no. 2, pp. 170–177, 2010.
[14] C. T. Nguyen, H.-S. Joo, J. Moon, and H.-E. Lee, "Flexural-torsional buckling strength of I-girders with discrete torsional braces under various loading conditions," *Engineering Structures*, vol. 36, pp. 337–350, 2012.
[15] E. Mohammadi, S. S. Hosseini, and M. S. Rohanimanesh, "Elastic lateral-torsional buckling strength and torsional bracing stiffness requirement for monosymmetric I-beams," *Thin-Walled Structures*, vol. 104, pp. 116–125, 2016.
[16] W. F. Zhang, *Out-of-Plane Stability Theory of Steel Structures*, Wuhan University of Technology Press, Wuhan, China, 2018, in Chinese.
[17] G. S. Tong, *Out-Plane Stability of Steel Structures*, China Architecture and Building Press, Beijing, China, 2006, in Chinese.
[18] J. Chen, *Stability of Steel Theory and Design*Science Press, Beijing, China, 6th edition, 2014, in Chinese.
[19] H. Achref, M. Foudil, and B. Cherif, "Higher buckling and lateral buckling strength of unrestrained and braced thin-walled beams: analytical, numerical and design approach applications," *Journal of Constructional Steel Research*, vol. 155, pp. 1–19, 2019.
[20] W. F. Zhang, "New engineering theory for torsional buckling of steel-concrete composite I-columns," in *Proceedings of the 11th International Conference on Advances in Steel and Concrete Composite Structures*, vol. 12, pp. 225–232, Beijing, China, 2012.
[21] W. F. Zhang, "Energy variational model and its analytical solutions for the elastic flexural-torsional buckling of I-beams with concrete-filled steel tubular flanges," in *Proceedings of the 8th International Symposium on Steel Structures*, pp. 1100–1108, Jeju, South Korea, 2006.
[22] W. F. Zhang, "New engineering theory for mixed torsion of steel-concrete-steel composite walls," in *Proceedings of 11th International Conference on Advances in Steel and Concrete Composite Structures*, vol. 12, pp. 705–712, Beijing, China, 2010.
[23] K. S. Chen, *Theoretical Research on Combined Torsion and Flexural-Torsional Buckling of the I-Shaped Beams with Concrete-Filled Steel Tubular Flange Based on the Plate-Beam Theory*, Northeast Petroleum University, Daqing, China, Master dissertation, 2017.
[24] W. F. Chen and E. M. Lui, *Structural Stability-Theory and Implementation*, Elsevier Science Publishing Co., Inc., New York, NY, USA, 1st edition, 1987.
[25] P. Z. Bazant and L. Cedolin, *Stability of Structures-Elastic, Inelastic, Fracture, and Damage Theories*, Oxford University Press, New York, NY, USA, 1991.
[26] W.-F. Zhang, Y.-C. Liu, K.-S. Chen, and Y. Deng, "Dimensionless analytical solution and new design formula for lateral-torsional buckling of I-beams under linear distributed moment via linear stability theory," *Mathematical Problems in Engineering*, vol. 2017, Article ID 4838613, 23 pages, 2017.
[27] W.-F. Zhang, "Symmetric and antisymmetric lateral-torsional buckling of prestressed steel I-beams," *Thin-walled Structures*, vol. 122, pp. 463–479, 2018.
[28] S. Kitipornchai, C. M. Wang, and N. S. Trahair, "Buckling of monosymmetric I-beams under moment gradient," *Journal of Structural Engineering*, vol. 112, no. 4, pp. 781–799, 1986.
[29] C. M. Wang and S. Kitipornchai, "Buckling capacities of monosymmetric I-beams," *Journal of Structural Engineering*, vol. 112, no. 11, pp. 2373–2391, 1986.
[30] GB/T3094, "The cold drawn shaped steel tubes," 2012.
[31] B. G. Kim and R. Sause, *Study of Two-Span Continuous Tubular Flange Girder Demonstrat-Ion Bridge*, Lehigh University, Bethlehem, Palestine, 2008.
[32] X. M. Wang, *Numerical Analyses of ANSYS Engineering Structure*, China Communications Press, Beijing, China, 2007.
[33] ANSYS APDL Programmer's Guide. Ansys Inc, 2004.
[34] M. F. Hassanein and N. Silvestre, "Lateral-distortional buckling of hollow tubular flange plate girders with slender unstiffened webs," *Engineering Structures*, vol. 56, pp. 572–584, 2013.